

Reactivity Manipulation of Ionic Liquid Based on Alkyl Primary Ammonium: Protonation Control Using Pyridine Additive for Effective Spontaneous Passivation of Perovskite via Hole Transport Material Deposition

Naoyuki Nishimura[†], Hiroaki Tachibana[†], Ryuzi Katoh[§], Hiroyuki Kanda[†], Takurou N. Murakami[†]*

[†] National Institute of Advanced Industrial Science and Technology (AIST), 1-1-1 Higashi, Tsukuba, Ibaraki 305-8565, Japan.

[§] College of Engineering, Nihon University, Koriyama, Fukushima 963-8642, Japan

*** Corresponding Author**

Naoyuki Nishimura. E-mail: naoyuki-nishimura@aist.go.jp

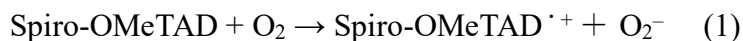
ABSTRACT

Alkyl-primary-ammonium-based room-temperature ionic liquids (RTILs) designed to exhibit specific reactivities allowing the functions that cannot be achieved by the current major RTILs (e.g., pyridine-based RTILs) have recently emerged. The archetype of the reactive RTILs is *n*-octylammonium bis(trifluoromethanesulfonyl)imide (OA-TFSI), which has promising functions as an additive for the hole transport material (HTM) in perovskite solar cells (PSCs); the high reactivity of the OA cations on the perovskite surface allows effective spontaneous perovskite passivation via HTM deposition, significantly improving the PV performance of the PSC. However, although the reactivity manipulation of the reactive RTILs is instrumental for exploiting their potential functions and exploring their application scope, methods for reactivity control have not been developed. In this study, we propose and demonstrate that the co-addition of a pyridine moiety can effectively manipulate the reactivity of OA-TFSI by controlling the protonation between OA and the 2,2',7,7'-tetrakis-(*N,N*-di-4-methoxyphenylamino)-9,9'-spirobifluorene (Spiro-OMeTAD) HTM. The pyridine prevented OA deprotonation presumably via stabilization of the OA cation, thus retaining its ammonium form, which allowed effective spontaneous perovskite passivation. Although the proton being with OA owing to pyridine addition is disadvantageous for Spiro-OMeTAD radical formation via its protonation, which is crucial when conventional RTILs are used, a supportive function of the spontaneous perovskite passivation (i.e., the absence of cationic species in the HTM core) likely facilitated Spiro-OMeTAD radical formation, mitigating the requirement of Spiro-OMeTAD protonation. Therefore, overall, optimal pyridine addition significantly enhanced the PV performance, revealing the preference of protonation in the OA-TFSI system used in this study, which is opposite to that in conventional RTILs and represents the specificity of the reactive RTILs. This study provides valuable guidance

for developing spontaneous perovskite passivation techniques, which can lead to further advancement of PCSs. Furthermore, this first proposal of a means in manipulating reactivity of the reactive RTILs will develop the nascent RTILs and contribute to further development of material science.

INTRODUCTION

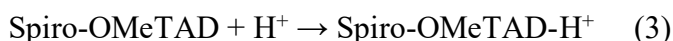
Perovskite solar cells (PSCs) have emerged as promising candidates for next-generation photovoltaics since a demonstration of their relatively high power-conversion efficiency (PCE) of ~10% in 2012.^{1,2} The standard configuration of a PSC comprises a transparent conductor, an electron transport material, a perovskite photoabsorber, a hole transport material (HTM), a metal conductor; a typical example of a PSC is fluorine-doped tin oxide (FTO)/titanium oxide (TiO₂)/perovskite/2,2',7,7'-tetrakis-(*N,N*-di-4-methoxyphenylamino)-9,9'-spirobifluorene (Spiro-OMeTAD)/Au). Significant advances have been achieved in the photovoltaic (PV) performances of PSCs in the past decade. For further PCS development, the obviation of Li species as an additive for organic semiconductor HTMs is a promising target as it can be detrimental to PSC performance.³⁻¹⁰ The major HTMs in PSCs are organic semiconductors (e.g., Spiro-OMeTAD); however, these pristine HTMs do not possess sufficient hole mobilities. Thus, additives for obtaining sufficient hole mobilities are generally employed for HTMs. The most typical additive is lithium bis(trifluoromethylsulfonyl)imide (Li-TFSI). The TFSI anions lead to the stabilization of the cationic HTM radicals (Equation 2) following radical formation via oxidation (e.g., Equation 1) that enhances the hole mobility of the HTM layer into the HTM solution.⁹⁻¹³



Nevertheless, the Li counter cations of TFSI in Li-TFSI are unnecessary for enhancing the hole mobility of the HTM; rather, they are considered to be detrimental to PV performance.³⁻¹⁰

Therefore, the replacement of Li-TFSI with other HTM additives is desired. Room-temperature ionic liquids (RTILs) have been proposed as promising HTM additives that do not contain Li

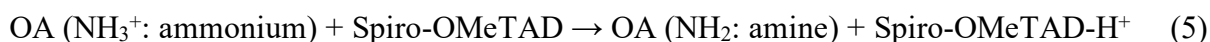
species.¹⁴⁻²⁴ At present, major RTILs comprise cations of imidazoles, pyridines, and quaternary-ammoniums, so these avoid the use of Li cations. In addition, notably, using RTILs based on cations that possess protons (e.g., imidazoles and pyridines), their protons can expediate the formation of HTM cation radicals via the protonation of the HTM (Equation 3 followed by Equation 4),¹⁴⁻²² which can be advantageous for obtaining efficient PCSs.



Very recent progress of RTIL additive for HTM is an alkyl-primary-ammonium TFSI (the archetype: *n*-octylammonium TFSI: OA-TFSI) possessing the reactivity allowing spontaneous perovskite passivation via HTM deposition process.^{23, 24} RTILs based on alkyl-primary-ammonium are diverging from the current main trend of the RTIL cation in the pursuit of applications such as electrolytes. Although such applications prefer moderate reactivities, this deviation of the RTIL composition enables specific functions to capitalize on the prominent cation's reactivity. In the case of OA-TFSI, by exploiting the high adsorption energy of OA cations on a perovskite surface (e.g., 1.88 eV²⁵), OA cations spontaneously passivate the perovskite during the deposition of an HTM solution containing the OA-TFSI additive.^{23, 24} As a result, the defects over the perovskite surface is effectively suppressed by the spontaneous passivation; thus, the use of OA-TFSI additive enhances the PV properties of PCSs without the conventional post-passivation process.^{23, 24}

However, as these spontaneous perovskite passivators (i.e., alkyl-primary-ammonium TFSI^{23, 24, 26}) is nascent, their mechanisms involving the manipulation of cation reactivities have remained elusive. A key to the efficient spontaneous perovskite passivation would be protonation control

among components of HTM solution. While the high adsorption energy of the ammonium form of OA can be advantageous for efficient spontaneous perovskite passivation, the protonation of the HTM via the deprotonation of OA to an amine form (Equation 5) can also be beneficial for HTM radical formation, as demonstrated for other RTIL additives.



Accordingly, both cases (i.e., protons with OA or Spiro-OMeTAD) may be beneficial for the PV performance of PCSs. Therefore, understanding the role of protonation in this system and the development of methods for protonation control will provide crucial insights into the spontaneous perovskite passivation mechanism and characteristics of the reactive RTILs (i.e., alkyl-primary-ammonium TFSIs).

In this study, we reveal that the co-addition of a pyridine derivative is instrumental for reactivity manipulation of an OA-TFSI RTIL via protonation control among components of an HTM solution. Owing to the presence of sufficient pyridine moiety in the HTM solution, the deprotonation of OA cations is hampered most likely via stabilization of its ammonium moiety, thereby allowing effective spontaneous perovskite passivation by OA effectively enhancing the PV performance of PCSs (Figure 1). Meanwhile, a deficit of the pyridine resulted in the inefficient perovskite passivation, most likely owing to the deprotonation of OA cations, in addition to the issue of affinity between the HTM solution and OA-TFSI, leading to low PV performances. Therefore, to exploit the alkyl-primary-ammonium TFSI additive for HTM, retaining the ammonium form of the cation is substantially more important than HTM protonation, unlike in the case of conventional RTILs (Figure 1). This work represents the importance of the reactivity control of cations in alkyl-primary-ammonium-based RTILs and can contribute to the further

development of spontaneous perovskite passivation for PCSs and the expansion of the application scope of RTILs.

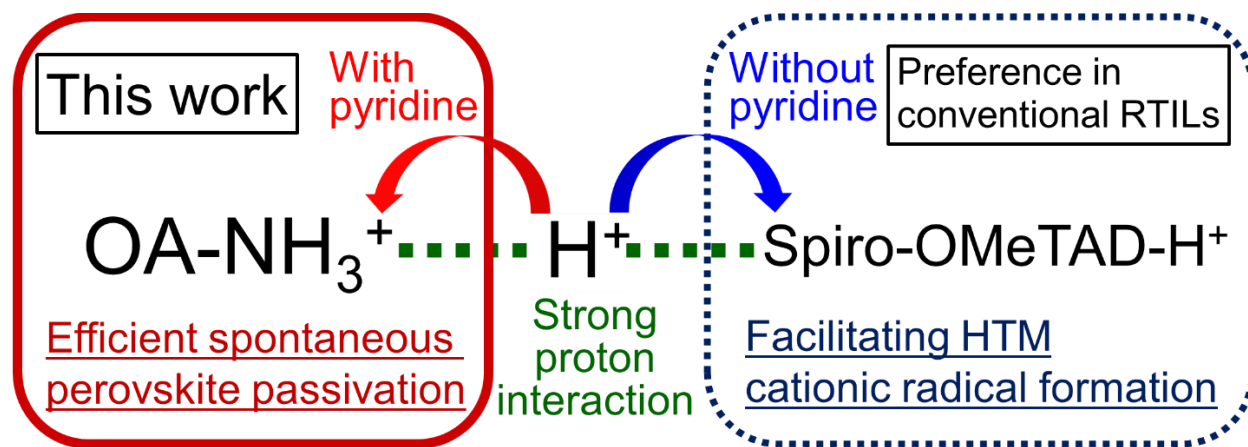


Figure 1. Scheme of the reaction manipulation of OA-TFSI via protonation control upon pyridine addition between the OA cation and Spiro-OMeTAD

EXPERIMENTAL SECTION

Synthesis of OA-TFSI

OA-TFSI was synthesized using a neutralization method²⁶ as follows. Ethanol solutions of *n*-octylamine and HTFSI with the same volumes and concentrations were prepared. The *n*-octylamine solution was then gradually added dropwise to the HTFSI solution while stirring in an ice bath. After stirring for 2 h, the ethanol was removed by a vacuum evaporator over 3 h. The resultant liquid was confirmed as OA-TFSI using NMR spectroscopy (Figure S1).

Solar Cell Fabrication

The PSCs were prepared along the conventional methods^{23, 26, 27} with some modifications. A compact layer of TiO₂ (50 nm) was coated onto an FTO glass substrate, which was then heated on a hotplate at 523 K, using spray pyrolysis from a 4 vol% titanium diisopropoxide bis(acetylacetonate)/ethanol solution. A mesoporous TiO₂ (m-TiO₂) layer was applied by spin coating a diluted TiO₂ paste in ethanol onto the substrate at 5000 rpm for 10 s, followed by annealing at 773 K for 30 min. An FA_{0.95}MA_{0.05}Pb(I_{0.95}Br_{0.05})₃ perovskite layer was deposited on the prepared TiO₂/FTO by spin coating in a dry room (temperature: 291 K, dew point: <243 K). The perovskite precursor solution was prepared by dissolving 1.72 M FAI, 86 mM MABr, 1.81 M PbI₂, 86 mM PbBr₂, and 0.69 M MACl in a mixed solution of *N,N*-dimethylformamide and dimethyl sulfoxide (volume ratio = 4:1). The TiO₂/FTO substrate was spin-coated with this solution at 6000 rpm for 50 s. During spin coating, chlorobenzene (0.5 mL) was added dropwise after 10 s of spinning. The HTM layer was deposited by spin coating a solution containing Spiro-OMeTAD and additives at 3000 rpm for 30 s in a dry room. The HTM solution with OA-TFSI was prepared by dissolving 70 mM Spiro-OMeTAD in chlorobenzene (CB) and mixing in the desired amounts of OA-TFSI and pyridine. 4-*tert*-butylpyridine (TBP)²⁸⁻³⁶ was used as the pyridine co-additive. TBP is commonly used for dissolving Li-TFSI solid salt in HTM solutions yet possesses specific roles in the system utilizing OA-TFSI. For the HTM solution with conventional additives, 70 mM Spiro-OMeTAD, 35 mM Li-TFSI, 0.23 mM TBP, and 4.2 mM FK209 were dissolved in CB and spin-coated at 4000 rpm for 30 s. Finally, a gold (Au) conductor layer (thickness ~200 nm) was deposited via thermal evaporation.

Current–Voltage Curve Measurement

Current–voltage (I–V) curves were obtained using a source meter (R6243, ADVANTEST) and a class A solar simulator (XIL-05B100KP, Seric Co.) with a mismatch factor below 25%, calibrated with an Si-reference cell equipped with a KG-5 filter to generate AM1.5G sunlight (100 mW cm^{-2}) at a room temperature of approximately 298 K in ambient atmosphere. The I–V scan was performed at a constant rate of 100 mV s^{-1} under simulated sunlight employing a sample mask to define an aperture area of 0.119 cm^2 . An antireflection sheet was applied to the glass side of the cell before each measurement, and no pre-bias was set prior to the measurements. Out of more than 18 samples tested under each condition, the best performers were selected for reporting. The average properties of the solar cells were then calculated. Stability tests were conducted more than 12 cells for set at $30 \text{ }^\circ\text{C}$ (303 K) with a relative humidity of 50%, without encapsulating the samples.

TRMC Measurement

Time-resolved microwave conductivity (TRMC) measurements^{23, 26, 37-43} utilized a custom-built setup. A Nd^{3+} :YAG laser (VN-200-10-ST, VM-TIM) generating the second harmonic (532 nm) served as the excitation source. Detailed information on the experimental arrangement is documented elsewhere.^{37, 39}

Characterizations of PCSs and Their Components

Cross-sectional scanning electron microscopy (SEM) images were acquired with an SEM system (SU9000; Hitachi). X-ray photoelectron spectroscopy (XPS) analyses were conducted using a QuanteraSXM (PHI Co.). $^1\text{H-NMR}$ spectra were measured with a Bruker AVANCE III HD 600 MHz spectrophotometer in deuterated chloroform (CDCl_3) or tetrahydrofuran ($\text{THF-}d_8$). Ionization potential of HTMs were measured by photoelectron yield spectroscopy (PYS; BIP-KV100H, Bunkou Keiki). The samples for wettability studies were prepared by depositing a perovskite layer onto an m-TiO₂/FTO substrate, followed by HTM deposition, mirroring the cell fabrication process. After assembling the bilayer samples, the HTM layer was removed by washing the samples with 0.7 mL of chlorobenzene (CB) 40 times, totaling 28 mL of CB. The wettability of the perovskite layer was assessed using a contact angle meter (Kyowa Interface Science Co.; DMO-401), equipped with a syringe fitted with either a pristine stainless steel (SUS; $\Phi 0.47$ mm) or a Teflon-coated needle, in a nitrogen atmosphere. A 1 μL droplet of a liquid was placed on the tested layers, and the contact angle (CA) between the droplet and layer was measured after 1 s. CA values were determined from the average of eight measurements, and error bars were estimated using the standard deviation.

RESULTS AND DISCUSSION

This study investigated the spontaneous passivation effects of OA-TFSI on a perovskite photoabsorber ($\text{FA}_{0.95}\text{MA}_{0.05}\text{Pb}(\text{I}_{0.95}\text{Br}_{0.05})_3$; 1.56 eV, [Figure S2](#)), which is wider-bandgap than the conventional photoabsorber used for the spontaneous perovskite passivation (≈ 1.53 eV)^{23, 24, 43}, and examined the impact of pyridine addition on the spontaneous passivation mechanism in PSC fabrication afterwards. [Figure 2](#) compares the PV performance of PSCs with the conventional set

of additives (i.e., Li-TFSI + FK209 + TBP) and the optimal amount of OA-TFSI + TBP additive (optimization: [Figure S3](#)). The samples with optimal 24 mM OA-TFSI (target) possessed significantly higher PV parameters than those with conventional additives (reference). Specifically, the PCE increased to 22.1% when using OA-TFSI, as shown in [Figure 2b](#) and [Table 1](#) (average PCE in backward scan: $20.6 \pm 0.7\%$; [Figure 2a](#) and [Table S1](#)), in relation to that of the samples with the conventional additive (highest PCE: 19.1%, average PCE in backward scan: $17.7 \pm 1.6\%$). This high performance is mainly due to the enhanced open-circuit voltage (V_{oc}), which represents the spontaneous perovskite passivation by the OA cations derived from the OA-TFSI additive. We note that J_{sc} in the J–V curve of the highest-performance cells (reference: 24.5 mA cm^{-2} , target: 24.8 mA cm^{-2}) matched well with the integrated J_{sc} estimated from the external quantum efficiency (EQE) curves (reference: 24.3 mA cm^{-2} , target: 24.9 mA cm^{-2}) within 1%. In addition to the J–V-curve-based performance, the quasi-steady-state PCE (QSS-PCE) of the OA-TFSI sample (21.4%) had a value similar to the PCE in the backward scan of the J–V curve, which was significantly higher than that of the sample with the conventional additive (18.0%).

The spontaneous passivation effects were further investigated. The presence of OA cations on the perovskite surface prepared using OA-TFSI was confirmed by XPS^{23, 44, 45} ([Figure S6](#)). Taking advantage of hydrophobicity of OA moiety over perovskite surface, the PCSs with OA-TFSI exhibited superior long-term stability in the presence of humidity (303 K with 50% relative humidity; [Figure S7](#)). In addition, the suppression of carrier traps on the perovskite surface through spontaneous passivation was examined using TRMC^{23, 26, 37-43} ([Figure S8](#)). TRMC has been reported as an effective method for investigating the carrier trap characteristics of the heterointerface between the HTM and perovskite in PSCs.^{23, 26} This method allows the detection of the lifetime of electrons in the perovskite after hole injection from the perovskite to the HTM

because hole mobility in the HTM is negligible in relation to that in the perovskite material. Thus, TRMC decay indicates changes in the carrier trap characteristics at the heterointerface between the HTM and perovskite when different HTM additives, such as Li-TFSI or OA-TFSI, are used (see SI for further details). The sample with OA-TFSI exhibited a substantially longer lifetime of electrons in the perovskite ($84 \pm 2 \mu\text{s}$) than that with the conventional additive ($4.6 \pm 0.1 \mu\text{s}$). Moreover, the excitation power dependence on TRMC decay (Figure S9) supports the suppression of the carrier traps using OA-TFSI. While the TRMC lifetime of the sample with Li-TFSI was reduced with increased excitation power, the sample with OA-TFSI exhibited a longer lifetime with increased excitation power. This trend strongly suggests that spontaneous perovskite passivation by the OA cations decreased the electron trap concentration at the HTM/perovskite interface, and the limited electron traps were adequately suppressed by the excited electrons in the employed excitation range.^{23, 26, 40} Therefore, it can be concluded that spontaneous passivation with OA-TFSI is effective for the employed perovskite photoabsorber ($\text{FA}_{0.95}\text{MA}_{0.05}\text{Pb}(\text{I}_{0.95}\text{Br}_{0.05})_3$: 1.56 eV). Based on these results, the effects of pyridine addition combined with OA-TFSI spontaneous passivation were explored using this photoabsorber.

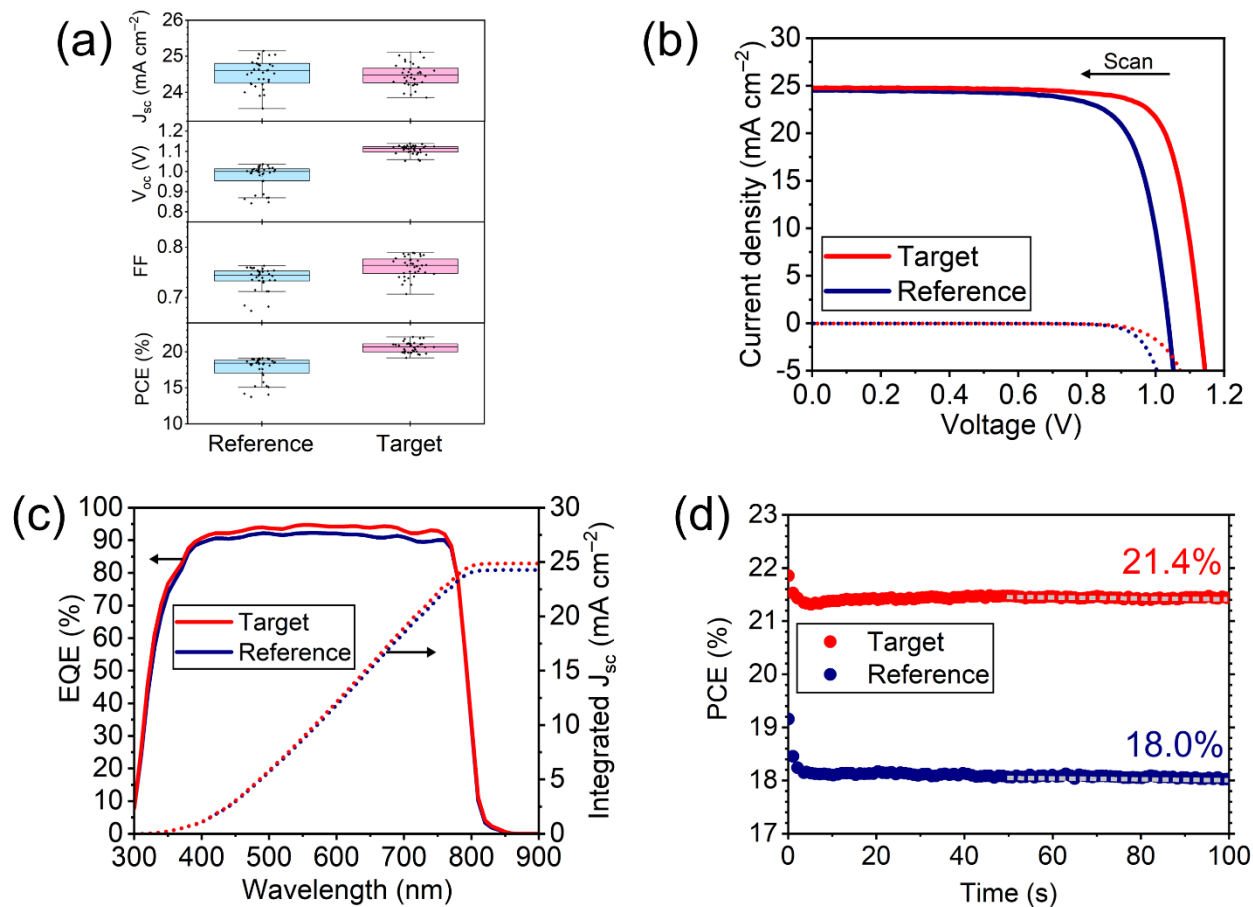


Figure 2. PV properties of PCSs with conventional HTM additives (reference) and the optimal OA-TFSI additive (target): (a) distributions of PV parameters in backward scan (forward scan: Figure S4), (b) J–V curves of the highest-performance cells in backward scan (forward scan: Figure S5), (c) EQE spectra, and (d) QSS-PCEs (reference at 0.86 V, target at 0.93 V)

Table 1. PV parameters of the highest-performance cells

Sample	Scan	J_{sc} (mA/cm ²)	V_{oc} (V)	FF	PCE (%)
Target	Backward	24.8	1.13	0.79	22.1
	Forward	24.8	1.08	0.70	18.6
Reference	Backward	24.5	1.04	0.75	19.1
	Forward	24.6	0.97	0.66	15.7

Pyridine addition will control the chemical interaction among the components of the HTM solution, and thus, change the HTM morphology. Hence, the effects of the pyridine addition on the HTM morphology were investigated. [Figure 3a](#) displays the images of HTM layers with varying amounts of TBP additives on perovskite/TiO₂/FTO substrates. The HTM layer without pyridine addition (0 mM) exhibited non-uniform film formation. Introducing a small amount of TBP (18 mM) led to a relatively uniform film but resulted in void formation that was visible to the naked eye. Moreover, sufficient TBP (≥ 54 mM) resulted in almost uniform morphologies at the macroscale. These findings suggest that although OA-TFSI is an RTIL mixed with a Spiro-OMeTAD CB solution, resulting in a transparent and clear solution (i.e., it appears uniform), the affinity between them is low, causing non-uniform films without TBP. Therefore, it was determined that TBP addition is crucial for achieving uniformity in the HTM layer when using OA-TFSI additive with Spiro-OMeTAD HTM.

The amount of pyridine added also changed the cross-sectional morphology of the HTM layer. [Figures 3b](#) and [S10](#) present the cross-sectional SEM images at the macroscale and magnified scales, respectively. The SEM images reveal that the morphology of the HTM layer varied with the TBP

concentration, while the composite layers other than the HTM remained unchanged. Large voids appeared over the surface of the sample without TBP addition (i.e., the 0 mM TBP sample), correlating with the visible non-uniformity observed in [Figure 3a](#), likely owing to the poor affinity between OA-TFSI and the HTM solution. In particular, the NMR spectroscopy results, which are discussed in the following section, imply that the affinity of OA-TFSI and CB solvent was presumably poor as OA-TFSI and Spiro-OMeTAD interacted strongly. Therefore, under the HTM deposition process, the CB solvent might accumulate on the upper side of the HTM surface, following which the evaporation of this chunk of solvent could have led to the large void formation. Conversely, smooth morphology of HTM was observed in the 18 mM TBP. However, the addition of 54 mM TBP led to the formation of additional voids within the HTM bulk, and further increasing the TBP to 108 mM caused the voids to enlarge, likely owing to the evaporation of residual TBP during the HTM deposition process.^{31, 32} Although void formation raises concerns regarding potential negative effects on the PV performance of PSCs, these voids negligibly affected the PV performance, as discussed later.

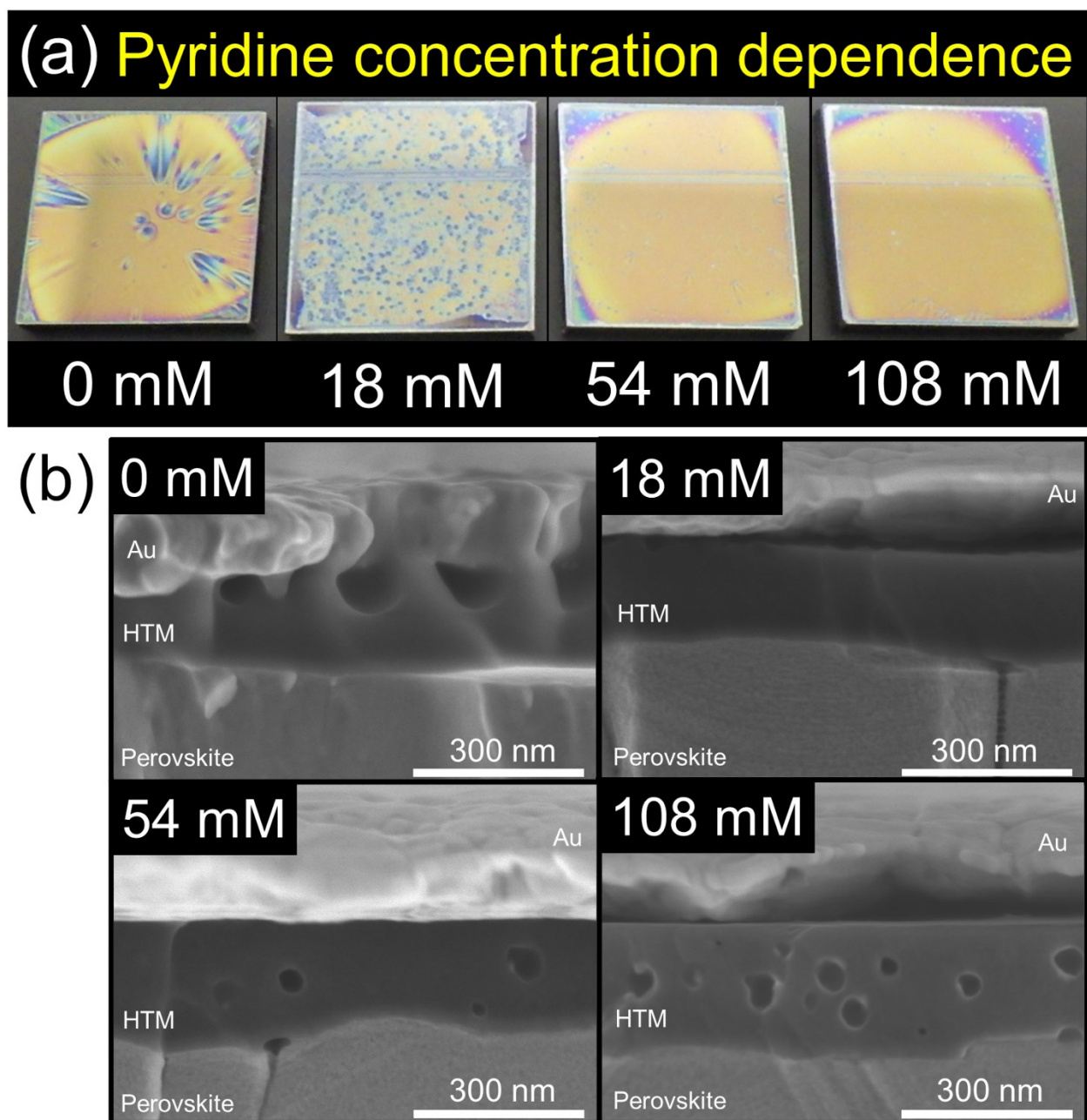


Figure 3. (a) Images of HTM layers with various concentrations of pyridine over perovskite layers and (b) cross-sectional images of PCSs using different concentrations of pyridine

Furthermore, chemical analysis revealed that pyridine addition plays crucial roles, not only in enhancing the affinity between OA-TFSI and the Spiro-OMeTAD solution but also in controlling protonation between the OA cations and Spiro-OMeTAD. [Figure 4](#) presents the $^1\text{H-NMR}$ spectra of the materials dissolved in deuterated THF. Solutions containing the individual materials of OA-TFSI and Spiro-OMeTAD exhibited distinct split peaks corresponding to each hydrogen atom ([Figures 4a](#) and [b](#); black lines). However, mixed solutions of OA-TFSI and Spiro-OMeTAD exhibited significantly different peak shapes ([Figures 4a](#) and [b](#); yellow lines), suggesting strong proton interaction between OA and Spiro-OMeTAD.^{14, 19} Meanwhile, further addition of TBP rendered the peak sharper ([Figures 4a](#) and [b](#); e.g., blue lines), suggesting prevention of the proton interaction between OA and Spiro-OMeTAD.

In further detail, although the two hydrogen atoms of the CH_2 moiety adjacent to the ammonium moiety (2H , t, CH_2NH_3) in OA are equivalent and should exhibit triplet NMR peaks, the pristine OA-TFSI sample exhibited multiple NMR peaks, similar to quintuple peaks. These observed quintuple-like peaks imply that parts of the ammonium moiety in the OA of individual OA-TFSI were deprotonated and existed in its amine form. In comparison, when Spiro-OMeTAD was added to OA-TFSI, this OA NMR peak was significantly broadened, suggesting a strong proton interaction between OA and Spiro-OMeTAD and anticipating the protonation of Spiro-OMeTAD (i.e., formation of Spiro-OMeTAD- H^+) via the deprotonation of OA. Indeed, the Spiro-OMeTAD cation radical, which was presumably formed via the protonation of Spiro-OMeTAD, was detected in the absorption spectrum at approximately 550 nm for the solution containing OA-TFSI and Spiro-OMeTAD,^{13, 14, 19} while the THF solution with only Spiro-OMeTAD did not exhibit the absorption derived from the cationic radical ([Figure S11](#)). However, addition of TBP to this mixture resulted in a sharper triplet NMR peak ([Figures 4a](#); e.g., blue lines), suggesting that

TBP hampered the strong proton interaction between OA and Spiro-OMeTAD. These triplet peaks with TBP addition strongly suggest that the prime chemical form of this functional group became the ammonium moiety—not amine—in contrast to OA-TFSI alone. Moreover, further addition of TBP shifted the triplet peaks farther from the original peaks (Figure 4a), suggesting that the OA ammonium interacted with TBP, and a higher concentration of TBP led to greater interaction between the OA cation and TBP. The absorption spectra were consistent with these NMR trends in terms of TBP addition; TBP addition to the OA-TFSI and Spiro-OMeTAD mixture solution substantially reduced the absorption at approximately 550 nm derived from the Spiro-OMeTAD cation radical (Figure S11), indicating the prevention of the protonation of Spiro-OMeTAD after deprotonation of the OA cation upon TBP addition.

Similar trends were observed in the NMR peaks corresponding to Spiro-OMeTAD (zoomed in: Figure 4b, wider scale: Figure S12). While the solution containing only Spiro-OMeTAD exhibited sharp peaks (the black line in Figure 4b), addition of OA-TFSI to Spiro-OMeTAD afforded a significantly broader peak (the yellow line in Figure 4b),^{14, 19} which is consistent with the NMR peaks of OA-TFSI (Figure 4a) and supports the strong proton interaction between OA and Spiro-OMeTAD. Further addition of TBP rendered the NMR peak sharper, similar to the original peaks, indicating prevention of proton interaction between Spiro-OMeTAD and OA-TFSI by TBP, as suggested by the NMR peak change of OA-TFSI (Figure 4a). Notably, with an increase in the TBP concentration, the NMR peak corresponding to Spiro-OMeTAD shifted to positions closer to those of the peaks of pristine Spiro-OMeTAD (Figure 4b). Combined to the trend of the OA-TFSI NMR peaks (e.g., the peak shift direction with increasing TBP concentration), hence, it can be concluded that TBP primarily interacted with the ammonium moiety of OA—not with Spiro-OMeTAD—and thus hampered the interaction between the OA cation and Spiro-OMeTAD.

The assumed interaction between OA and TBP may be due to the electronegativity of the nitrogen atom in TBP and/or the lone pair of electrons on the pyridine moiety, which could help stabilize the cationic OA ammonium moiety.

These observations strongly suggest that TBP addition can manipulate the reactivity of the alkyl-primary-ammonium RTILs via protonation control; TBP addition to the mixture controls and prevents the proton interactions between OA-TFSI and Spiro-OMeTAD, thereby maintaining the ammonium form of OA and hampering Spiro-OMeTAD protonation.

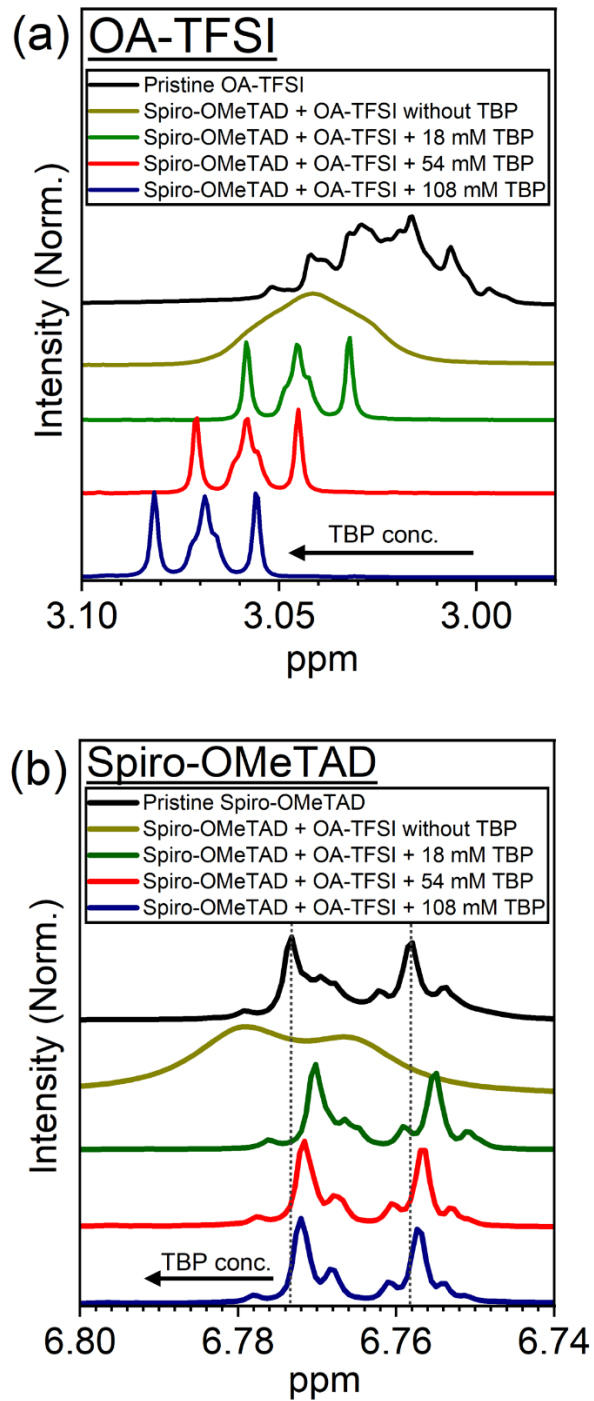


Figure 4. NMR spectra of pristine materials and mixtures of 70 mM Spiro-OMeTAD, 24 mM OA-TFSI, and various concentrations of TBP for (a) OA-TFSI (2H, t, CH₂NH₃) and (b) Spiro-OMeTAD (Figure S12: wider range and assignment)

As revealed above, TBP presumably stabilized OA cations and thereby most likely prevents the protonation of Spiro-OMeTAD following the deprotonation of OA-TFSI. That is, the TBP concentration presumably modulates the concentration of protonated Spiro-OMeTAD contributing to Spiro-OMeTAD cation radical formation (Equation 1). To explore the concentration modulation of the Spiro-OMeTAD cation radicals upon TBP addition, the ionization energies of the HTM layers were investigated (Figure 5a and Table S2). As the energy level of the SOMO correlating Spiro-OMeTAD cation radicals was deeper than the HOMO level of pristine Spiro-OMeTAD,⁹ larger ionization energy of the HTM layers suggests a higher concentration of Spiro-OMeTAD cation radicals. We note that the employed samples for the IP measurements were HTM/perovskite bilayer samples because it is appropriate to observe the IP of actual HTM, and HTM solutions containing OA-TFSI exhibit terribly poor wettability over substrates other than perovskite layers. Among the samples with various TBP concentrations, the HTM without TBP (0 mM) resulted in the deepest IP of 5.63 eV, most likely owing to the efficient protonation of Spiro-OMeTAD (Equation 3) without the prevention of TBP. With an increase in the TBP concentration to 18 and 54 mM, their IPs became slightly shallow, at 5.61 and 5.60 eV, respectively. With a further increase in the TBP concentration to 108 mM, the IP became significantly shallow, at 5.45 eV. This trend is presumably because (i) TBP hampered deprotonation of OA cation and thereby prevented Spiro-OMeTAD protonation, and/or (ii) the excess TBP addition led to higher concentration of the TBP uncoordinated to OA, and the free TBP prevented the Spiro-OMeTAD radical formation (and/or de-doping Spiro-OMeTAD cationic radical) as previously reported.³³⁻³⁵ Therefore, it is strongly suggested that TBP controls the protonation of Spiro-OMeTAD, thereby modulating the concentration of Spiro-OMeTAD cation radicals in the HTM.

Furthermore, retaining the ammonium form of OA (i.e., protons with OA) via the prevention of deprotonation by TBP would be advantageous for effective perovskite passivation. Thus, TRMC measurements were performed on samples with varying TBP concentrations to explore the spontaneous passivation effects of OA cations in suppressing carrier traps between the HTM and perovskite. [Figure 5b](#) depicts the TRMC decay for the sample using optimal OA-TFSI with different TBP concentrations, and [Table 2](#) outlines the estimated lifetimes of the TRMC signal with single exponential fitting. The inclusion of 18 mM ($88 \pm 2 \mu\text{s}$) and 54 mM TBP ($84 \pm 2 \mu\text{s}$) significantly extended the electron lifetime from the sample without TBP ($5.3 \pm 0.1 \mu\text{s}$), which is attributable to the passivation effects of OA cations. The similar TRMC lifetime of the sample without TBP ($5.3 \pm 0.1 \mu\text{s}$) to the sample with conventional additive ($4.6 \pm 0.1 \mu\text{s}$, [Figure S8](#)) suggests that the deprotonated OA of the amine form possessed some function of perovskite passivation in suppressing defects. Moreover, the addition of excess TBP (108 mM) decreased the electron lifetime ($39 \pm 1 \mu\text{s}$), suggesting that excess TBP might obstruct perovskite passivation by OA. This obstruction of OA passivation by TBP presumably occurred because (i) the excess interaction between OA and TBP, which was observed in the NMR spectra ([Figure 4a](#)), decreased the passivator function of OA and/or (ii) the excess amount of TBP directly formed a chemical bond to the perovskite surface,^{28-30, 36, 46} thereby hampering effective passivation by OA cations. The excitation power dependence of the TRMC decays ([Figure S9 and S13](#)) also supports the effective perovskite passivation with the ammonium form of OA; only the sample without TBP addition (0 mM TBP) exhibited shorter TRMC lifetimes with increased excitation power, whereas other samples with TBP addition (i.e., 54 mM ([Figure S9](#)), and 18 and 108 mM ([Figure S13](#))) showed longer TRMC lifetimes with increased excitation power. This trend is most likely owing to the limited concentration of carrier traps following effective passivation with the ammonium

form of OA via the prevention of deprotonation by TBP addition.^{23, 26, 40} Consequently, the TRMC measurements revealed that OA in the ammonium form with TBP assistance was significantly effective in suppressing defects over the perovskite surface via spontaneous passivation, whereas OA without TBP, which presumably induced the deprotonation of OA to its amine form, was slightly effective in canceling the carrier traps.

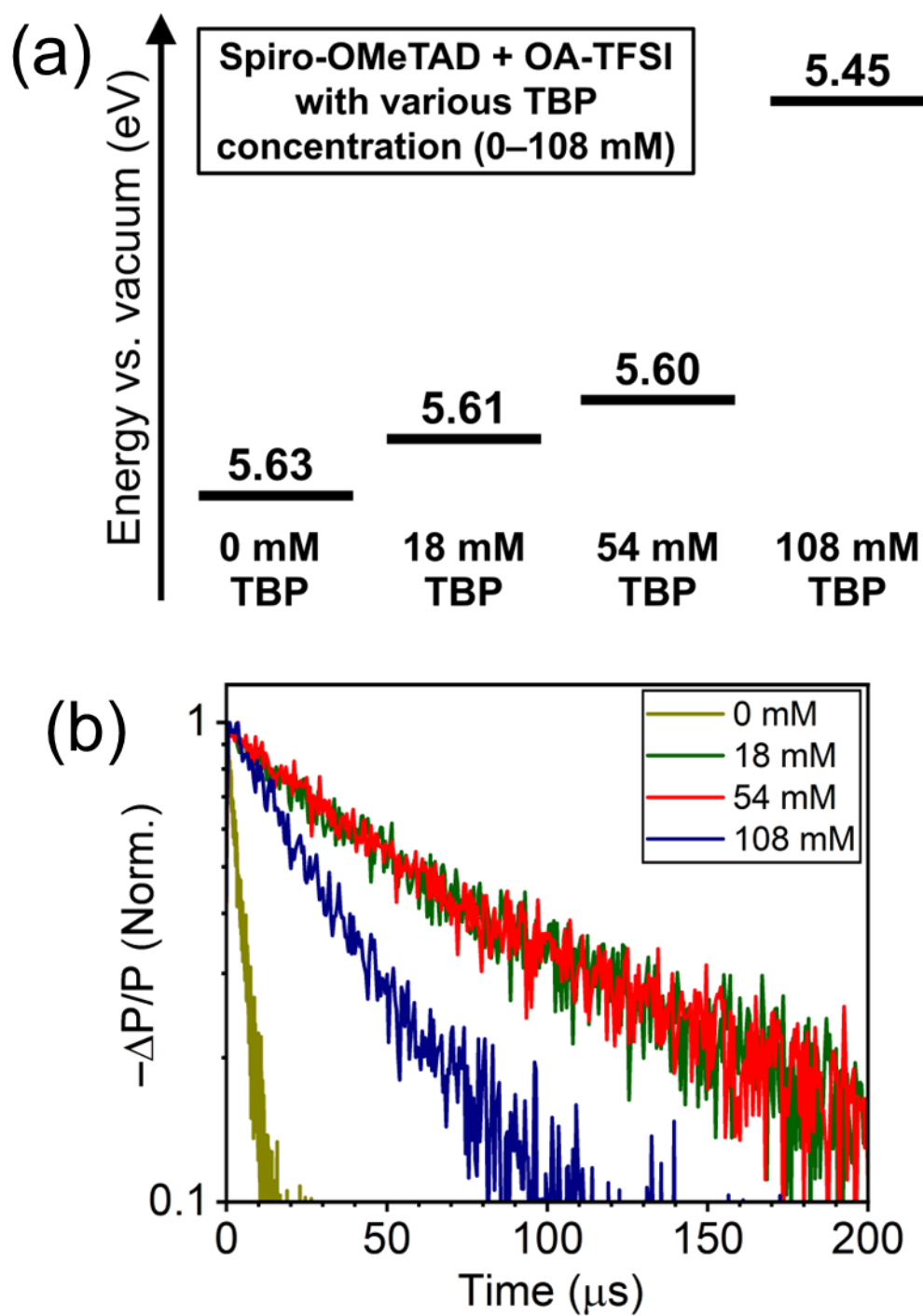


Figure 5. (a) summary of IP measurement (b) TRMC signal decay of HTM/perovskite bilayer sample with HTM additive of 24 mM OA-TFSI and various concentrations of TBP

Table 2. Lifetimes of TRMC signals

TBP concentration (mM)	Lifetime (μs)
0	5.3 ± 0.1
18	88 ± 2
54	84 ± 2
108	39 ± 1

Thus far, it has been demonstrated that TBP addition is advantageous for effective perovskite passivation, whereas it is disadvantageous for the formation of Spiro-OMeTAD cation radicals. Hence, the TBP concentration dependence on the PV properties is of interest. Figure 6 showcases the PV performance of PSCs with optimal OA-TFSI and varying TBP concentrations (0 to 108 mM). The backward scans of the J–V curves reveal a notable increase in the PCE with increasing TBP concentrations from 0 to 54 mM, both on average (from $12.0 \pm 1.6\%$ to $20.9 \pm 0.8\%$, as shown in Figure 6a and Table S3) and for the highest-performance cells (from 13.7% to 22.1%, as detailed in Figure 6b and Table 3). This improvement in PCE is credited to increases in the open-circuit voltage (V_{oc}) from 0.97 to 1.13 V and fill factor (FF) from 0.58 to 0.79 in the highest-performance cells. This V_{oc} enhancements likely represent the effects of perovskite passivation and are in line with the TRMC trend (Figure 5b and Table 2); only the 0 mM TBP sample resulted in a considerably shorter TRMC lifetime ($5.3 \pm 0.1 \mu\text{s}$, compared to $84 \pm 2 \mu\text{s}$ of the 54 mM TBP sample). Moreover, the improved uniformity of the HTM layer at the macroscale presumably contributed to the FF enhancement, aligning with the observations in Figure 3a. However, further increasing the TBP to 108 mM slightly decreased the PCE (e.g., highest-performance cell PCE:

21.2%), accompanied by a decrease in V_{oc} (from 1.13 to 1.09 V). This V_{oc} decrease is consistent with the observed trends in the TRMC decay; an excess of 108 mM TBP reduced the TRMC lifetime presumably because excess TBP hampered perovskite passivation by OA cation (Figure 5 and Table 2). The forward scans exhibited similar trends. In terms of the EQE measured (Figure S16), regardless of similar J_{sc} values in the J–V curves among the PCSs, only the 0 mM TBP sample exhibited substantially low values (J_{sc} in the J–V curve: 24.2 mA cm^{-2} , integrated J_{sc} from the EQE spectrum: 23.1 mA cm^{-2}) compared with the PCSs with sufficient TBP (e.g., 54 mM), suggesting that HTM deposition without TBP led to the formation of defects, thereby deviating from the linearity of the current–excitation density relationship. The QSS-PCEs (Figure 6c) also mirrored the J–V curve trends; with an increase in TBP from 0 to 54 mM, the QSS-PCE increased from 12.2% to 21.4%, and then decreased to 20.2% with a further TBP increase to 108 mM.

Apart from the initial PV performance, the observed void formation in the HTM core with TBP addition (Figure 4b) raises concerns regarding stability against humidity; the presence of voids in the HTM core could allow humidity to penetrate the HTM layer more easily, potentially reaching the perovskite layer more frequently. To explore the impact of these voids in the HTM, a stability test under conditions of 50% relative humidity at 303 K (30 °C) was conducted on PSCs with varying amounts of TBP addition (18 mM: non-voids, 54 and 108 mM: plenty of voids). It is noteworthy that the perovskite surfaces of these samples exhibited similar hydrophobicity, as determined by contact angle measurements with water droplets over the samples after removal of the HTM layers (Figure S17), owing to the OA passivation effects. Figure S18 shows the results of the stability test. Remarkably, none of the samples exhibited a performance drop in 1500 h, even with voids present in the HTM layer, for additions of 54 and 108 mM TBP. This trend indicates that the presence of voids in the HTM layer owing to substantial TBP addition did not have a

significant impact on stability against humidity; rather, hydrophobicity of the perovskite surface presumably determined stability against humidity in this series of PSCs. Thus, the presence of voids in the HTM layer caused by TBP addition was not found to be detrimental to the PV performances.

Consequently, the present findings strongly suggest that the optimal addition of TBP in controlling protonation between OA and Spiro-OMeTAD is instrumental in enhancing PV performance by harnessing the spontaneous passivation potential of OA-TFSI. While excess TBP may interfere with perovskite passivation by OA cations, the resultant formation of voids in the HTM layer is not significantly detrimental to PV performance.

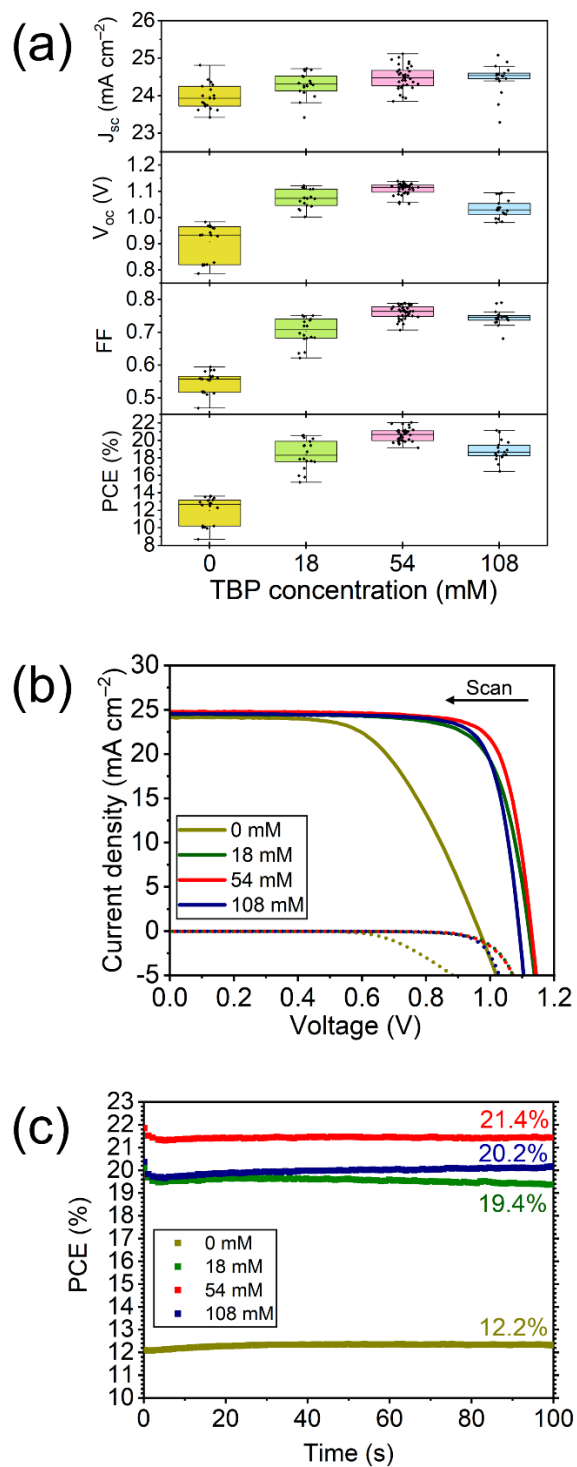


Figure 6. PV performance of PSCs with 24 mM OA-TFSI and TBP of 0, 18, 54, and 108 mM; (a) PV parameter distribution, (b) J-V curves in backward scan, (c) QSS-PCEs

Table 3. PV parameters of highest-performance cells with varying TBP concentrations

TBP concentration (mM)	Scan	J_{sc} (mA/cm ²)	V_{oc} (V)	FF	PCE (%)
0	Backward	24.2	0.97	0.58	13.7
	Forward	24.2	0.91	0.47	10.3
18	Backward	24.5	1.12	0.75	20.6
	Forward	24.5	1.09	0.68	18.0
54	Backward	24.8	1.13	0.79	22.1
	Forward	24.8	1.08	0.70	18.6
108	Backward	24.5	1.09	0.79	21.2
	Forward	24.6	1.04	0.74	18.9

Finally, as the preferable protonation trend in the present OA-TFSI RTIL may contradict that in the case of other RTIL additives for the HTM¹⁴⁻²², the specificity of OA-TFSI RTIL is discussed. Although for other HTM additives of RTILs, the protonation of Spiro-OMeTAD via the deprotonation of the RTIL cations was instrumental for exploiting their functions in facilitating Spiro-OMeTAD radical formation,¹⁴⁻²² the present RTIL (i.e., OA-TFSI) resulted in the opposite trend: the protons on the OA cations and not on Spiro-OMeTAD was substantially more beneficial (Figure 1). This is presumably not only because of the significance of the effective perovskite passivation, but also owing to another function of this spontaneous perovskite passivator: the absence of counter cations of the TFSI-based additive in the HTM core, facilitating Spiro-

OMeTAD cation radical formation and stabilization with TFSI anions.²³ Under the spontaneous perovskite passivation using OA-TFSI, the OA cations spontaneously migrated and passivated to the perovskite layer, and thus, the OA cations were absent in the HTM core.^{23, 26} As the Spiro-OMeTAD cation radical formation is relevant to charge transfers from pristine Spiro-OMeTAD to electron accepters (e.g., O₂ molecule in [Equation 1](#)), the presence of cationic species in the HTM core most likely hampers Spiro-OMeTAD cation radical formation. In addition, the stabilization of Spiro-OMeTAD cation radicals with TFSI anions can be prevented by the presence of cationic species. Thus, the absence of cations in the HTM core following spontaneous perovskite passivation will be beneficial for increasing Spiro-OMeTAD cation radical concentrations. Indeed, in the present results, the IPs of HTMs with OA-TFSI, even with a lower TFSI concentration (24 mM) and obstructed protonation of Spiro-OMeTAD by TBP, resulted in significantly deeper IPs (5.45 – 5.63 eV) than that of the HTM with the conventional additive (39 mM TFSI concentration, 5.15 eV: [Table S2](#)). The observed deeper IPs using OA-TFSI supports that occurrence of the facilitation Spiro-OMeTAD radical formation took advantage of the absence of counter cations in HTM core.

Therefore, in the case of OA-TFSI, by exploiting the function of facilitating Spiro-OMeTAD radical formation other than the protonation of Spiro-OMeTAD, the requirement of Spiro-OMeTAD protonation is mitigated, resulting in the protonation preference different from the conventional RTIL additives; the presence of protons on OA cations is significant for enhancing the PV performance of PCSs. In other words, the mitigated requirement of Spiro-OMeTAD protonation, elucidated in this work, supports the proposed mechanism of facilitated Spiro-OMeTAD radical formation exploiting the absence of cation species in the HTM core.

CONCLUSION

This study proposed a means of reactivity control of the reactive RTILs for the first time and demonstrated that manipulating the reactivity of the cations in alkyl-primary-ammonium TFSI is vital for effective spontaneous perovskite passivation via HTM deposition. Particularly, the co-addition of a pyridine moiety to the OA-TFSI additive for the Spiro-OMeTAD HTM solution can help manipulate the reactivity of the OA cations by controlling the protonation between OA and Spiro-OMeTAD (Figure 1).

Without pyridine (TBP) co-addition, strong proton interaction occurred between OA and Spiro-OMeTAD. Although Spiro-OMeTAD cation radical formation was facilitated by the protonation of Spiro-OMeTAD, OA deprotonated to the amine form, leading to inefficient spontaneous perovskite passivation via HTM deposition and thus poor PV performance. However, the addition of a sufficient amount of TBP hampered the deprotonation of OA cations, presumably via stabilization of the ammonium moiety by TBP for retaining the ammonium form, in addition to improving the affinity between OA-TFSI and the HTM solution. Therefore, spontaneous perovskite passivation proceeded effectively, improving the PV performance. Meanwhile, the addition of excess TBP obstructed spontaneous perovskite passivation by OA, presumably via the chemical attachment of TBP over perovskite and/or excessively strong interaction between TBP and OA cations.

The preference of protonation in the RTIL used in this study (i.e., OA-TFSI) contradicts that for other HTM additives of conventional RTILs (Figure 1): the protons on Spiro-OMeTAD are crucial for facilitating cation radical formation in terms of exploiting conventional RTIL additives. This difference can be attributed to the function of OA-TFSI in facilitating HTM radical formation

by a means other than the protonation of Spiro-OMeTAD (i.e., the absence of counter cations of RTILs in the HTM core), obviating Spiro-OMeTAD protonation.

The insights obtained from this study can contribute to the development of a promising method for spontaneous perovskite passivation via HTM deposition using alkyl-primary-ammonium TFSI. Moreover, the insights regarding protonation effects on HTM composites can lead to a more profound understanding of HTM additives and the mechanism of HTM radical formation, contributing to further advancements in PSCs. Furthermore, the results demonstrate the importance of manipulating the reactivity of cations in alkyl-primary-ammonium-based RTILs and provide valuable guidance for exploring other applications of the recently emerged yet potent RTILs that exploit their specific reactivities.

Acknowledgements

This article is based on results obtained from a project, JPNP21016, commissioned by the New Energy and Industrial Technology Development Organization (NEDO).

Author contributions

Naoyuki Nishimura: Conceptualization, Project administration, Investigation, Resources, Formal analysis, Writing – original draft, Writing – review & editing, **Hiroaki Tachibana:** Investigation, Writing – review & editing, **Ryuzi Katoh:** Investigation, Writing – review & editing, **Hiroyuki Kanda:** Writing – review & editing, **Takuro N. Murakami:** Supervision, Funding acquisition, Writing – review & editing

Notes

There are no conflicts to declare.

References

- (1) Lee, M. M.; Teuscher, J.; Miyasaka, T.; Murakami, T. N.; Snaith, H. J. Efficient hybrid solar cells based on meso-superstructured organometal halide perovskites. *Science* **2012**, *338*, 643-647.
- (2) Kim, H. S.; Lee, C. R.; Im, J. H.; Lee, K. B.; Moehl, T.; Marchioro, A.; Moon, S. J.; Humphry-Baker, R.; Yum, J. H.; Moser, J. E.; et al. Lead iodide perovskite sensitized all-solid-state submicron thin film mesoscopic solar cell with efficiency exceeding 9%. *Sci. Rep.* **2012**, *2*, 591.
- (3) Li, Z.; Xiao, C.; Yang, Y.; Harvey, S. P.; Kim, D. H.; Christians, J. A.; Yang, M.; Schulz, P.; Nanayakkara, S. U.; Jiang, C.-S.; et al. Extrinsic ion migration in perovskite solar cells. *Energy Env. Sci.* **2017**, *10*, 1234-1242.
- (4) Dawson, J. A.; Naylor, A. J.; Eames, C.; Roberts, M.; Zhang, W.; Snaith, H. J.; Bruce, P. G.; Islam, M. S. Mechanisms of Lithium Intercalation and Conversion Processes in Organic–Inorganic Halide Perovskites. *ACS Energy Lett.* **2017**, *2*, 1818-1824.
- (5) Seo, J.-Y.; Kim, H.-S.; Akin, S.; Stojanovic, M.; Simon, E.; Fleischer, M.; Hagfeldt, A.; Zakeeruddin, S. M.; Grätzel, M. Novel p-dopant toward highly efficient and stable perovskite solar cells. *Energy Env. Sci.* **2018**, *11*, 2985-2992.
- (6) Tan, B.; Raga, S. R.; Chesman, A. S. R.; Furer, S. O.; Zheng, F.; McMeekin, D. P.; Jiang, L.; Mao, W.; Lin, X.; Wen, X.; et al. LiTFSI-Free Spiro-OMeTAD-Based Perovskite Solar Cells with Power Conversion Efficiencies Exceeding 19%. *Adv. Ener. Mater.* **2019**, *9*, 1901519.
- (7) Hu, M.; Wu, X.; Tan, W. L.; Tan, B.; Scully, A. D.; Ding, L.; Zhou, C.; Xiong, Y.; Huang, F.; Simonov, A. N.; et al. Solvent Engineering of a Dopant-Free Spiro-OMeTAD Hole-Transport Layer for Centimeter-Scale Perovskite Solar Cells with High Efficiency and Thermal Stability. *ACS Appl. Mater. Interfaces* **2020**, *12*, 8260-8270.
- (8) Zhang, Y.; Huang, B.; Hu, M.; Tan, B.; Huang, F.; Cheng, Y.-B.; Simonov, A. N.; Lu, J. Radical doped hole transporting material for high-efficiency and thermostable perovskite solar cells. *J. Mater. Chem. A* **2022**, *10*, 10604-10613.
- (9) Schloemer, T. H.; Christians, J. A.; Luther, J. M.; Sellinger, A. Doping strategies for small molecule organic hole-transport materials: impacts on perovskite solar cell performance and stability. *Chem. Sci.* **2019**, *10*, 1904-1935.
- (10) Rombach, F. M.; Haque, S. A.; Macdonald, T. J. Lessons learned from spiro-OMeTAD and PTAA in perovskite solar cells. *Energy Env. Sci.* **2021**, *14*, 5161-5190.
- (11) Cappel, U. B.; Daeneke, T.; Bach, U. Oxygen-induced doping of spiro-MeOTAD in solid-state dye-sensitized solar cells and its impact on device performance. *Nano Lett.* **2012**, *12*, 4925-4931.

- (12) Abate, A.; Leijtens, T.; Pathak, S.; Teuscher, J.; Avolio, R.; Errico, M. E.; Kirkpatrick, J.; Ball, J. M.; Docampo, P.; McPherson, I.; Snaith, H. J. Lithium salts as "redox active" p-type dopants for organic semiconductors and their impact in solid-state dye-sensitized solar cells. *Phys. Chem. Chem. Phys.* **2013**, *15*, 2572-2579.
- (13) Wang, S.; Yuan, W.; Meng, Y. S. Spectrum-Dependent Spiro-OMeTAD Oxidization Mechanism in Perovskite Solar Cells. *ACS Appl. Mater. Interfaces* **2015**, *7*, 24791-24798.
- (14) Abate, A.; Hollman, D. J.; Teuscher, J.; Pathak, S.; Avolio, R.; D'Errico, G.; Vitiello, G.; Fantacci, S.; Snaith, H. J. Protic ionic liquids as p-dopant for organic hole transporting materials and their application in high efficiency hybrid solar cells. *J. Am. Chem. Soc.* **2013**, *135*, 13538-13548.
- (15) Zhang, H.; Shi, Y.; Yan, F.; Wang, L.; Wang, K.; Xing, Y.; Dong, Q.; Ma, T. A dual functional additive for the HTM layer in perovskite solar cells. *Chem. Commun.* **2014**, *50*, 5020-5022.
- (16) Zhang, J.; Zhang, T.; Jiang, L.; Bach, U.; Cheng, Y.-B. 4-tert-Butylpyridine Free Hole Transport Materials for Efficient Perovskite Solar Cells: A New Strategy to Enhance the Environmental and Thermal Stability. *ACS Energy Lett.* **2018**, *3*, 1677-1682.
- (17) Caliò, L.; Salado, M.; Kazim, S.; Ahmad, S. A Generic Route of Hydrophobic Doping in Hole Transporting Material to Increase Longevity of Perovskite Solar Cells. *Joule* **2018**, *2*, 1800-1815.
- (18) Zhou, X.; Hu, M.; Liu, C.; Zhang, L.; Zhong, X.; Li, X.; Tian, Y.; Cheng, C.; Xu, B. Synergistic effects of multiple functional ionic liquid-treated PEDOT:PSS and less-ion-defects S-acetylthiocholine chloride-passivated perovskite surface enabling stable and hysteresis-free inverted perovskite solar cells with conversion efficiency over 20%. *Nano Energy* **2019**, *6319*.103866
- (19) Geffroy, C.; Grana, E.; Bessho, T.; Almosni, S.; Tang, Z.; Sharma, A.; Kinoshita, T.; Awai, F.; Cloutet, E.; Toupance, T.; et al. p-Doping of a Hole Transport Material via a Poly(ionic liquid) for over 20% Efficiency and Hysteresis-Free Perovskite Solar Cells. *ACS Appl. Energy Mater.* **2020**, *3*, 1393-1401.
- (20) Zhang, T.; Wang, F.; Kim, H. B.; Choi, I. W.; Wang, C.; Cho, E.; Konefal, R.; Puttisong, Y.; Terado, K.; Kobera, L.; et al. Ion-modulated radical doping of spiro-OMeTAD for more efficient and stable perovskite solar cells. *Science* **2022**, *377*, 495-501.
- (21) Niu, T.; Chao, L.; Gao, W.; Ran, C.; Song, L.; Chen, Y.; Fu, L.; Huang, W. Ionic Liquids-Enabled Efficient and Stable Perovskite Photovoltaics: Progress and Challenges. *ACS Energy Lett.* **2021**, 1453-1479.
- (22) Luo, J.; Lin, F.; Yuan, J.; Wan, Z.; Jia, C. Application of Ionic Liquids and Derived Materials to High-Efficiency and Stable Perovskite Solar Cells. *ACS Mater. Lett.* **2022**, *4*, 1684-1715.
- (23) Nishimura, N.; Tachibana, H.; Katoh, R.; Kanda, H.; Murakami, T. N. Archetype-Cation-Based Room-Temperature Ionic Liquid: Aliphatic Primary Ammonium Bis(trifluoromethylsulfonyl)imide as a Highly Functional Additive for a Hole Transport Material in Perovskite Solar Cells. *ACS Appl. Mater. Interfaces* **2023**, *15*, 44859-44866.
- (24) Kim, Y.; Kim, G.; Park, E. Y.; Moon, C. S.; Lee, S. J.; Yoo, J. J.; Nam, S.; Im, J.; Shin, S. S.; Jeon, N. J.; Seo, J. Alkylammonium bis(trifluoromethylsulfonyl)imide as a dopant in the hole-transporting layer for efficient and stable perovskite solar cells. *Energy Env. Sci.* **2023**, *16*, 2226-2238.
- (25) Tan, S.; Huang, T.; Yavuz, I.; Wang, R.; Weber, M. H.; Zhao, Y.; Abdelsamie, M.; Liao, M. E.; Wang, H. C.; Huynh, K.; et al. Surface Reconstruction of Halide Perovskites During Post-treatment. *J. Am. Chem. Soc.* **2021**, *143*, 6781-6786.

- (26) Nishimura, N.; Kanda, H.; Katoh, R.; Murakami, T. N. Thermally Stable Phenylethylammonium-based Perovskite Passivation: Spontaneous Passivation with Phenylethylammonium Bis(trifluoromethylsulfonyl)imide under Deposition of PTAA for Enhancing Photovoltaic Performances of Perovskite Solar Cells. *ChemRxiv* **2023**. DOI: 10.26434/chemrxiv-2023-0wrzg
- (27) Nishimura, N.; Mathew, S.; Murakami, T. N. Suppressing hydrogen bonds and controlling surface dipole: effective passivation for hydrophobic perovskite photoabsorber layers in solar cells. *New J. Chem.* **2023**, *47*, 4197-4201.
- (28) Noel, N. K.; Abate, A.; Stranks, S. D.; Parrott, E. S.; Burlakov, V. M.; Goriely, A.; Snaith, H. J. Enhanced photoluminescence and solar cell performance via Lewis base passivation of organic-inorganic lead halide perovskites. *ACS Nano* **2014**, *8*, 9815-9821.
- (29) Li, W.; Dong, H.; Wang, L.; Li, N.; Guo, X.; Li, J.; Qiu, Y. Montmorillonite as bifunctional buffer layer material for hybrid perovskite solar cells with protection from corrosion and retarding recombination. *J. Mater. Chem. A* **2014**, *2*, 13587-13592.
- (30) Yue, Y.; Salim, N.; Wu, Y.; Yang, X.; Islam, A.; Chen, W.; Liu, J.; Bi, E.; Xie, F.; Cai, M.; Han, L. Enhanced Stability of Perovskite Solar Cells through Corrosion-Free Pyridine Derivatives in Hole-Transporting Materials. *Adv. Mater.* **2016**, *28*, 10738-10743.
- (31) Wang, S.; Sina, M.; Parikh, P.; Uekert, T.; Shahbazian, B.; Devaraj, A.; Meng, Y. S. Role of 4-tert-Butylpyridine as a Hole Transport Layer Morphological Controller in Perovskite Solar Cells. *Nano Lett.* **2016**, *16*, 5594-5600.
- (32) Jena, A. K.; Ikegami, M.; Miyasaka, T. Severe Morphological Deformation of Spiro-OMeTAD in (CH₃NH₃)PbI₃ Solar Cells at High Temperature. *ACS Energy Lett.* **2017**, *2*, 1760- 1761.
- (33) Kim, J.; Park, N.; Yun, J. S.; Huang, S.; Green, M. A.; Ho-Baillie, A. W. Y. An effective method of predicting perovskite solar cell lifetime—Case study on planar CH₃NH₃PbI₃ and HC(NH₂)₂PbI₃ perovskite solar cells and hole transfer materials of spiro-OMeTAD and PTAA. *Solar Energ. Mater. Solar Cells* **2017**, *162*, 41-46.
- (34) Kasparavicius, E.; Magomedov, A.; Malinauskas, T.; Getautis, V. Long-Term Stability of the Oxidized Hole-Transporting Materials used in Perovskite Solar Cells. *Chem. Eur. J.* **2018**, *24*, 9910-9918.
- (35) Lamberti, F.; Gatti, T.; Cescon, E.; Sorrentino, R.; Rizzo, A.; Menna, E.; Meneghesso, G.; Meneghetti, M.; Petrozza, A.; Franco, L. Evidence of Spiro-OMeTAD De-doping by tert-Butylpyridine Additive in Hole-Transporting Layers for Perovskite Solar Cells. *Chem* **2019**, *5*, 1806-1817.
- (36) Tumen-Ulzii, G.; Auffray, M.; Matsushima, T.; Adachi, C. Unintentional passivation of 4-tertbutyl pyridine for improved efficiency and decreased operational stability of perovskite solar cells. *Appl. Phys.ics Lett.* **2021**, *118*, 0051527.
- (37) Katoh, R.; Furube, A.; Yamanaka, K.-i.; Morikawa, T. Charge Separation and Trapping in N-Doped TiO₂ Photocatalysts: A Time-Resolved Microwave Conductivity Study. *J. Phys. Chem. Lett.* **2010**, *1*, 3261-3265.
- (38) Oga, H.; Saeki, A.; Ogomi, Y.; Hayase, S.; Seki, S. Improved understanding of the electronic and energetic landscapes of perovskite solar cells: high local charge carrier mobility, reduced recombination, and extremely shallow traps. *J. Am. Chem. Soc.* **2014**, *136*, 13818-13825.
- (39) Nakajima, S.; Katoh, R. Time-resolved microwave conductivity study of charge carrier dynamics in commercially available TiO₂ photocatalysts. *J. Mater. Chem. A* **2015**, *3*, 15466-15472.

- (40) Hutter, E. M.; Hofman, J. J.; Petrus, M. L.; Moes, M.; Abellón, R. D.; Docampo, P.; Savenije, T. J. Charge Transfer from Methylammonium Lead Iodide Perovskite to Organic Transport Materials: Efficiencies, Transfer Rates, and Interfacial Recombination. *Adv. Ener. Mater.* **2017**, *7*, 1602349.
- (41) Petrus, M. L.; Schutt, K.; Sirtl, M. T.; Hutter, E. M.; Closs, A. C.; Ball, J. M.; Bijleveld, J. C.; Petrozza, A.; Bein, T.; Dingemans, T. J.; et al. New Generation Hole Transporting Materials for Perovskite Solar Cells: Amide-Based Small-Molecules with Nonconjugated Backbones. *Adv. Ener. Mater.* **2018**, *8*, 1801605.
- (42) Hempel, H.; Savenije, T. J.; Stolterfoht, M.; Neu, J.; Failla, M.; Paingad, V. C.; Kužel, P.; Heilweil, E. J.; Spies, J. A.; Schleuning, M.; et al. Predicting Solar Cell Performance from Terahertz and Microwave Spectroscopy. *Adv. Ener. Mater.* **2022**, *12*, 2102776.
- (43) Nishimura, N.; Behera, R. K.; Katoh, R.; Kanda, H.; Murakami, T. N.; Matsuzaki, H. Unveiled Effects of Methylammonium Chloride Additives on Formamidinium Lead Halide: Expediting Carrier Injection from the Photoabsorber to Carrier Transport Layers through Spontaneously Modulated Heterointerfaces in Perovskite Solar Cells. *ChemRxiv* **2024**. DOI: 10.26434/chemrxiv-2024-vhmzx.
- (44) He, M.; Liang, J.; Zhang, Z.; Qiu, Y.; Deng, Z.; Xu, H.; Wang, J.; Yang, Y.; Chen, Z.; Chen, C.-C. Compositional optimization of a 2D–3D heterojunction interface for 22.6% efficient and stable planar perovskite solar cells. *J. Mater. Chem. A* **2020**, *8*, 25831-25841.
- (45) Akin, S.; Dong, B.; Pfeifer, L.; Liu, Y.; Graetzel, M.; Hagfeldt, A. Organic Ammonium Halide Modulators as Effective Strategy for Enhanced Perovskite Photovoltaic Performance. *Adv. Sci.* **2021**, *8*, 2004593.
- (46) Habisreutinger, S. N.; Noel, N. K.; Snaith, H. J.; Nicholas, R. J. Investigating the Role of 4-Tert Butylpyridine in Perovskite Solar Cells. *Adv. Ener. Mater.* **2016**, *7*, 1601079.